Catal Lett (2007) 119:311–318
DOI 10.1007/s10562-007-9237-z

NH_3 Decomposition Kinetics on Supported Ru Clusters: Morphology and Particle Size Effect

Weiqing Zheng · Jian Zhang · Hengyong Xu · Wenzhao Li

Received: 1 July 2007 / Accepted: 1 August 2007 / Published online: 15 August 2007

Abstract The supported Ru clusters with mean sizes ranging from 1.9 to 4.6 nm showed a high activity towards the NH_3 decomposition reaction. The structural properties of catalysts were characterized by N_2 adsorption/desorption, X-ray diffraction (XRD) and transmission electron micrograph (TEM). Steady-state reaction kinetics revealed that the apparent activation energy increased with a decrease in Ru particle size and ranged from 79 kJ mol^{-1} to 122 kJ mol^{-1}. The decomposition rate over Ru nanoparticles showed a strong dependency on mean crystallite size and the optimum appeared at d_{Ru} = 2.2 nm. The dependencies of reaction rate on partial pressures of NH_3 and H_2 were also sensitive to the varying Ru particle size. Experimental data could be well fitted by the Temkin–Pyzhev equation, indicating that the recombinative desorption of surface nitrogen atom acts as the rate-determining step. A compensation effect between the pre-exponential factor (k_0) and activation energy (E_a) was quantified.

Keywords Ammonia decomposition · Ru · Kenitics · Size effects · Compensation effect

1 Introduction

Catalytic decomposition of NH_3 provides an applicable route to CO_x-free H_2 stream for the fuel cell uses. Over the past few years, the NH_3 decomposition process has been extensively studied mainly driving by either the scientific view to get insight into the mechanism of NH_3 synthesis [1, 2] or the technological opinion to use liquid NH_3 as a suitable H_2 carrier [3–5]. It has been reported that group VIII metals (Fe, Ni, Ru, Ir, Co, Pt) catalyze the NH_3 decomposition reaction and Ru is generally considered to be the most active single metal catalysts [6–9]. Ru-CeO_2/Y Zeolite [2], Ru/Al_2O_3 [6, 8], Ru/SiO_2 [6, 10], Ru/C [11–15], Ru/$MgAl_2O_4$ [9, 16], Ru/CNTs [8, 10, 15, 17], and Ru/MgO [8, 10, 17, 18] have been proved to catalyze decomposition of NH_3.

Although the assessments of relevant elementary steps and structure sensitivity in NH_3 decomposition have been widely reported, the kinetics of NH_3 decomposition over Ru is not well established and many contradictory findings still remain unresolved. Tsai and Weinberg [19] investigated the kinetics of NH_3 dissociation over Ru (001) plane. The authors found that the rate determining step (RDS) changed with the temperature and established a reaction expression under the hypothesis that both the recombinative desorption of N* as the most abundant reactive intermediate (MARI) and the initial N–H bond cleavage are slow elementary steps. However, their expression could not describe the H_2 inhibition phenomenon that was widely observed in the later studies. In contrast, Tamaru [20, 21] proposed that there was a quasi-equilibration among N*, gaseous NH_3 and H_2 and recombinative desorption of N* determined the decomposition rate, which was proved by the further studies of Vitvitski [22] and Mariadassou [23]. Such model could be represents as followed:

$$2NH_3(g) + 2* \overset{k_1}{\Leftrightarrow} 2N* + 3H_2(g) \quad \text{(i)}$$

$$2N* \overset{k_2}{\rightarrow} N_2(g) + 2* \quad \text{(ii)}$$

Bradford [11] studied the kinetics over Ru nanoparticles at 623–723 K and reported that the decomposition of NH_3 is

W. Zheng · J. Zhang · H. Xu (✉) · W. Li
Dalian Institute of Chemical Physics, Graduate School of the Chinese Academy of Sciences, Dalian 116023, China
e-mail: xuhy@dicp.ac.cn

0.69–0.75 order in NH_3 and −2 to −1.6 order in H_2, and both NH_2–H bond cleavage and recombinative nitrogen desorption (Eq. 2) are slow kinetic steps, which sustained by the obtained good statistical fit to experimental data. Most recently, based on the results of microkinetic model with the unity bond index–quadratic exponential potential (UBI–QEP), Mhadeshwar predicated that the RDS in NH_3 decomposition is the N–H bond cleavage in NH_2* while the recombinative desorption of nitrogen contributes much less to the overall reaction rate [24]. Moreover, there are some apparent discrepancies in the surface science studies over Ru surface, either the experimental observations or theoretical calculations. Great differences in operation conditions, from UHV to high pressures (atm level), and samples, from single crystal to supported catalyst, should be sufficiently considered. In addition, the adsorbate–adsorbate interactions always considerably change the RDS, MARI and the maximum coverage of N*, which also leads to the different conclusion in kinetically significant steps in literature [24].

Many papers have suggested that the rates of N_2 dissociation and NH_3 decomposition are strongly sensitive to the concentration of one special assemble of metal atoms, such as C-7 sites on Fe and B-5 sites on Ni and Ru. Single crystal studies and density function theory (DFT) calculations for Ni and Ru revealed that the maximum probability for B-5 sites appeared for particles of 1.5–2.5 nm [25–27]. Jedynak et al. observed that smaller particles of Fe over K–Fe/C catalysts possessed higher turnover frequencies (TOFs) and attributed the reason to higher concentration of C-7 sites over the more highly dispersed catalyst [27]. When studied the NH_3 decomposition on Ru crystallites, Li et al. found less activity of the extra-small Ru particles (d_{Ru} = 1.6 nm) [15]. However, there is lack of the experimental evidence from the direct correlation between intrinsic activity and crystallite size of supported Ru clusters. Furthermore, supports are often found to strongly influence NH_3 decomposition rate on Ru crystallites, whereas their effects on the dispersion of active phase and mass transport artifacts have rarely been discussed [6–8], which might result in the great discrepancies existing among the previous studies.

In present study, we will report a successful synthesis of highly active Ru/Al_2O_3 catalysts for NH_3 decomposition. The XRD and TEM characterizations of the reduced samples revealed the mean sizes of Ru^0 crystallites over a series of catalysts with different metal loading. The kinetic behavior of them will be conducted in a fix-bed differential reactor, in which the transport artifacts were ruled out. Influence of Ru crystal size on catalytic activity toward NH_3 decomposition will be detailed. Then, we will try to investigate the kinetically controlled step by correlation between experimental data with a kinetic model.

2 Experimental Section

2.1 Synthesis of Ru Catalysts

A series of Ru/Al_2O_3 with different Ru loading (Table 1) were prepared by incipient wetness impregnation of Al_2O_3 with an ethanol solution of $RuCl_3 \cdot xH_2O$ (Jiushan Chemical Corp., Shanghai, China, 99.99%). The Al_2O_3 support (276 $m^2\ g^{-1}$) was synthesized by using a coprecipitation method as described by us previously [28]. Aluminum nitrate [$Al(NO_3)_3 \cdot 9H_2O$] and ammonium carbonate [$(NH_4)_2CO_3$] with stoichiometric molar ratios were separately dissolved in double de-ionized water. Over a period of 2 h, both aqueous solutions were added simultaneously to a glass beaker with vigorous stirring. The precipitate was aged in the mother liquor, removed, washed thoroughly with double de-ionized water, and the obtained solid was dried in air at 383 K overnight, and successively calcined at 873 K for 5 h. The massive sample was then ground into the fine powder.

The synthesis procedures of Ru/Al_2O_3 catalysts comprised conventional impregnation at 353 K for 8 h, drying at 393 K in ambient air overnight and then calcination in a muffle by increasing the temperature to 833 K (2 K min^{-1}) and holding for 5 h. The obtained mass solids were washed by $NH_3 \cdot H_2O$ (4 M) at 353 K for 6 h, dried in air overnight, crushed and sized into the particle of 100–150 μm. BET surface areas of all calcined samples were illustrated in Table 1.

2.2 Catalytic Measurements

Ru/Al_2O_3 samples (100 mg) were loaded between two quartz wool plugs in a conventional quartz reactor and then treated by 50% H_2 in He (100 $cm^3\ min^{-1}$) at 833 K (2 K min^{-1}) for 5 h. Pure ammonia with a space velocity of 30,000 mL/g_{cat} h was used as the reactant for the conventional catalytic evaluations. Temperature of the catalyst bed was detected by a movable K-type thermocouple enclosed with quartz sheath. Flow rates of gases were controlled by the mass flowmeters (Brooks). Product analysis was carried out with an on-line gas chromatograph (Shimadzu 8A) with a Porapak-N column and a TCD detector.

The kinetic evaluations were performed in a fix-bed differential quartz reactor using catalyst pellets (10 mg) diluted with inert quartz powder (500 mg) to prevent temperature gradients. Typically, the reactants mixtures consisted of 15% anhydrous NH_3 and 85% He with a total space velocity of 3,000,000 mL $g_{cat}^{-1}\ h^{-1}$ and NH_3 conversion were less than 20%. The influence of NH_3 pressure on reaction rates was determined over a wide range of

Table 1 Sample characterizations by BET, H_2-Chemisorption, XRD and TEM

Sample	State	SA (m^2/g)	SA_{Ru} [a] (m^2/g)	Surface Ru atoms[a] (mol/g)	d_{RuO_2} (nm)	d_{Ru} (nm)	
					XRD	XRD	TEM
0.7 wt.%Ru/Al_2O_3	Reduced	–	0.24	3.73×10^{19}	4.8	4.4	1.9
1.9 wt.%Ru/Al_2O_3	Reduced	239	0.39	6.06×10^{19}	8.4	7.5	2.2
2.9 wt.%Ru/Al_2O_3	Reduced	221	0.54	9.51×10^{19}	8.1	6.8	2.9
4.7 wt.%Ru/Al_2O_3	Reduced	192	–	–	7.9	7.2	3.5
5.7 wt.%Ru/Al_2O_3	Reduced	–	–	–	7.9	7.2	4.2
7.0 wt.%Ru/Al_2O_3	Reduced	182	–	–	7.9	8.7	4.6
Al_2O_3	–	276	–	–	–	–	–

Calculation based on the irreversible H_2 adsorption amount obtained from the chemisorption isotherm at 303 K

partial pressure from 10 kPa to 50 kPa. The N_2 and H_2 dependencies were measured at 5–40 kPa while the NH_3 pressure maintaining at 15 kPa.

2.3 Catalyst Characterization

Surface areas were measured by N_2 physisorption using a Micromeritics ASAP 2010P apparatus and standard multipoint BET analysis methods. H_2 adsorption was performed to estimate surface area of Ru. The intercept of the total irreversible at zero pressure was used and an H_s/Ru ratio of 1.0 was assumed. Prior to each test, the catalyst was reduced in by H_2–He mixture at 833 K for 5 h, swept by ultrapure He for 2 h, and then cooled down to 303 K in evacuation. Powder X-ray diffraction patterns were obtained at room temperature using a Philips diffractometer and CuK_α radiation. The metal particle size and dispersion were determined from TEM microscopes obtained with a Philips Tecnai G2 T20ST transmission electron microscope. The materials were placed on a carbon-coated copper grid and measured with a maximum acceleration voltage of 200 kV. The crystal size distribution was estimated by measuring the size of 100–200 of the nanometer-sized features.

3 Results and Discussion

3.1 Catalytic Activity for NH_3 Decomposition

The conversion as a function of temperature was determined for each catalyst and presented in Fig. 1. Catalytic tests were performed under the atmospheric pressure and pure NH_3 was used as the reactant. Obviously, the synthesized Ru/Al_2O_3 catalysts showed high reactivity towards the NH_3 decomposition reaction. At the temperature higher than 823 K, all catalysts except 0.7%Ru/Al_2O_3 could almost completely decomposed NH_3 with the space

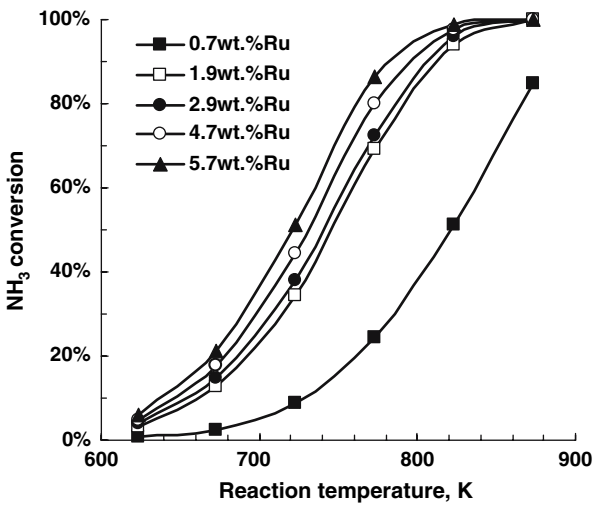

Fig. 1 Temperature-dependent NH_3 conversion over catalysts with varying Ru loading. Reaction conditions: SV_{NH_3} = 30,000 mL g_{cat}^{-1} h^{-1}, catalysts loading 100 mg, 623–873 K

velocity of 30,000 h^{-1}. It is as expected that the reactivity increased with the Ru loading. For example, at 773 K, the NH_3 conversion over 0.7%Ru/Al_2O_3 and 1.9%Ru/Al_2O_3 were 23% and 68%, respectively. However, with further increasing Ru loading to 5.7%, there was no significant increase in reactivity, suggesting a loss in usage of the active phase.

A comparison of H_2 formation rate between our catalysts and the ones reported in literature was listed in Table 2. It is clearly seen that, under the same reaction condition, our Ru/Al_2O_3 is more active than the other Ru/Al_2O_3 in literature and comparable with the Ru/CNT catalyst whose activity was believed to be the highest. Furthermore, as evidenced in Table 2, the impregnation prepared Ru catalysts by using organic substances (e.g. ethanol, acetone) as the solvent always possessed a high activity. Such results revealed that the reactivity of Ru catalyst would be strongly influenced by various factors, such as the preparation condition, support, metal dispersion, etc. It is therefore suggested that when the

Table 2 H_2 formation rate ($mmolH_2\ g_{cat}^{-1}\ min^{-1}$) over various supported Ru catalysts. Condition: pure NH_3, SV_{NH_3} = 30,000 mL $g_{cat}^{-1}\ h^{-1}$, 100 mg catalyst

Sample	Solvent	Dispersion[a] (%)	Temperature (K)			Reference
			673	773	873	
10%Ru/Al_2O_3	Water	2.8	4.5	18.1	24.7	6
10%Ru/SiO_2	Water	1.2	4.5	20.0	30.3	6
4.8%Ru/Al_2O_3	Water	6.0	0.6	5.6	–	17
4.8%Ru/Al_2O_3	Acetone	10.0	3.9	16.5	–	17
4.8%Ru/MgO	Acetone	8.8	5.4	23.5	–	17
4.8%Ru/AC	Acetone	20.6	3.8	21.5	–	17
4.8%Ru/CNT	Acetone	21.1	5.7	28.4	–	17
4.7%Ru/Al_2O_3	Ethanol	28.6[b]	5.9	26.8	33.5	This study

[a] Calculated from the adsorption data in H_2 chemisorption experiments

[b] Calculated from the TEM result

effect of a particular factor is discussed, all other parameters should be fixed unchanged.

3.2 Transmission Electron Microscopy (TEM)

The metal loading has a great impact on the final morphology of the alumina-supported Ru nanoparticles. TEM images and particle size distributions of three typical reduced samples are shown in Fig. 2. Obviously, most of the Ru is present in the form of particles with diameters below 5 nm. Some bigger particles appeared in images of the samples with high metal loading, indicating somewhat sintering of the active phase during the thermal pretreatments. For instance, the crystallites up to a diameter of 16 nm were found in the images of 7.0%Ru/Al_2O_3 sample. For all samples, the particle size distribution is generally monomodal with a maximum ranging from 1.9 nm to 4.6 nm. The higher the Ru content, the wider the distribution of particle size.

3.3 X-ray Diffraction (XRD)

The comparative X-ray diffraction patterns of the calcined and reduced catalysts are presented in Fig. 3. The diffraction features at Bragg angles of 28.1, 35.1 and 54.3° revealed the presence of RuO_2 crystallites in calcined samples while those of 38.4, 42.1, 44.0, 58.3, 69.4 and 78.3° indicated the existence of Ru crystallites in reduced samples. With increasing metal loading, the diffraction peaks became more intensive but the mean sizes of RuO_2 and Ru that calculated from the Bragg equation did not changed. As listed in Table 1, the values of d_{RuO_2} and d_{Ru} ranged at 8.0 and 7.0 nm, respectively. The difference between XRD and TEM could be interpreted by the limited detection level of XRD technique. In XRD determination, the particles with size smaller than 2–3 nm that possessed a high particle fraction could not be detected. Therefore, the mean sizes of Ru obtained from XRD were much higher than those obtained from TEM.

3.4 Reaction Kinetics

To investigate the reaction mechanism, the kinetics measurements were performed. All the forward reaction rates were corrected for approach to equilibrium (η) from thermodynamic data. The value of $(1 - \eta)$ is larger than 0.998 for all catalytic measurements reported here. Note that the forward rate (r_f) were obtained from $r_{net} = (r_f - r_r) = r_f(1 - \eta)$, in which r_{net} represents the net reaction rate.

3.4.1 Particle Size Effect

Figure 4 reports the steady-state activities of the prepared Ru catalysts for NH_3 decomposition at 733 K as a function of metallic Ru crystallite size. The forward reaction rates increased with particle size to a maximum i.e., 2,210 $g_{NH_3}\ g_{Ru}^{-1}\ h^{-1}$, at the mean size of 2.2 nm followed with by a decline in activity with a further increase in size. Figure 4 also shows a strong particle size effect on the forward turnover rate (TOF_{NH_3}), which reveals a significant structural sensitivity for NH_3 decomposition over the supported Ru nanoparticles. The catalytic performance for ammonia decomposition could benefit for the high loading of Ru. Actually, in the conventional impregnation method, the severe sintering of Ru could not be successfully prevented, even though various high-surface-area supports (e.g. active carbon, carbon nanotubes) and some organic solvents as the dispersion media have been used [6–8, 18]. Large metal particles possess extremely low intrinsic activity, which would cause a sharp loss in effective utilization of noble metal. It is an important issue how to synthesize the supported Ru nanoparticles with mean size at around 2.2 nm and narrow particle size distribution. A powerful support for the particle size effect

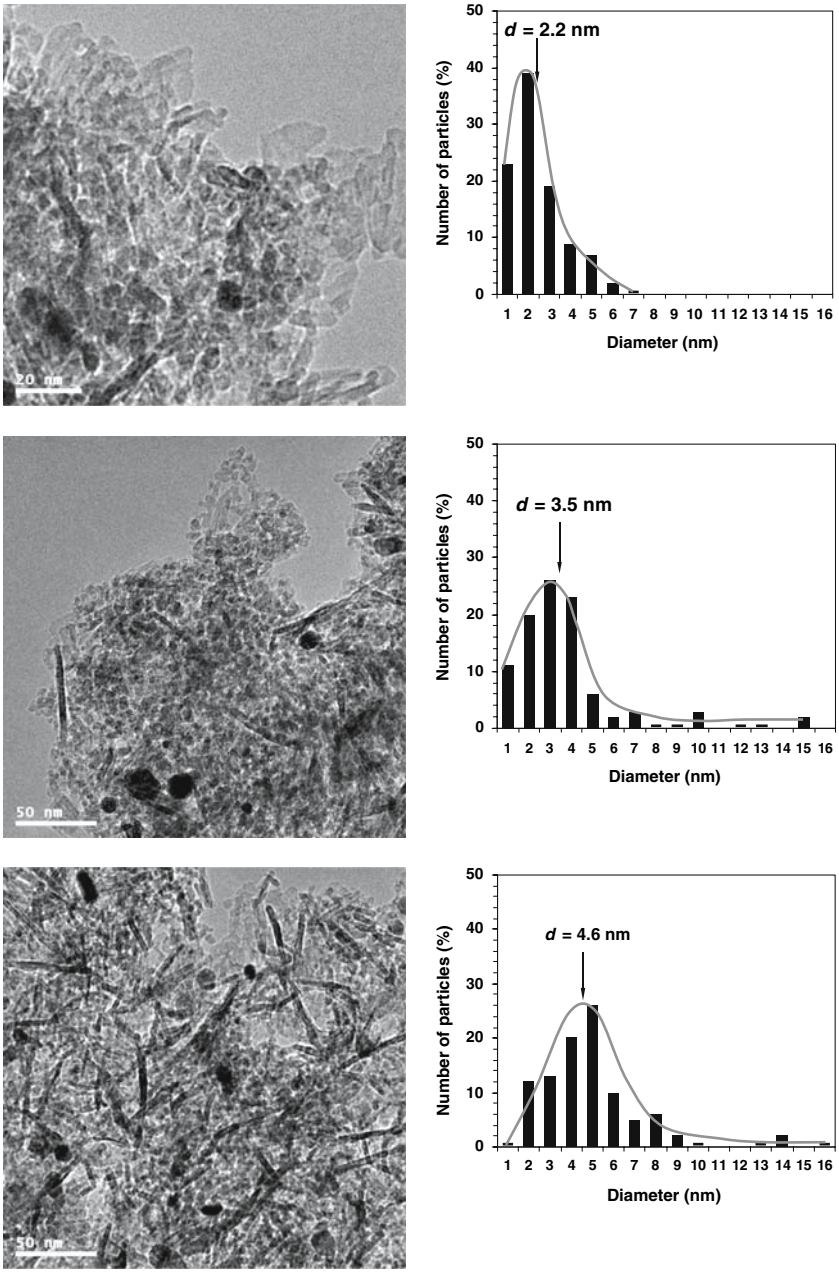

Fig. 2 Selected TEM images and particle size distributions of the reduced samples. (**a**) 1.9 wt.% Ru (2.2 nm); (**b**) 4.7 wt.% Ru (3.5 nm); (**c**) 7.0 wt.% Ru (4.6 nm)

is our recent success in novel synthesis of MgO-supported Ru nanoparticles (d = 1.2–2.3 nm, $d_{average}$ = 2.0 nm) that possessed an outstanding activity for NH_3 decomposition while compared with those in literature [29].

Figure 5 shows the apparent activation energy (E_a) for NH_3 decomposition at 653–733 K as a function of Ru crystallite diameter. Clearly, the energies ranged from 80 kJ mol^{-1} to 123 kJ mol^{-1} and decreased with the crystallite size. These variances of both reaction rate and activation energy with the changing Ru particle size suggested a pronounced structure sensitivity of NH_3 decomposition over the supported Ru nanoparticles.

For the curves of reactivity versus particle size pass through a maximum in the range of around 2–3 nm, the B-5 sites, i.e. five atoms exposing a three-fold hollow *hcp* site and a bridge site close together, have often been proposed as the active centers for other reactions [30, 31]. In the calculation results describing the arrangement of the atoms in small crystallites, Hardeveld and Montfoort [26] have reported that, for a Ni crystal of octahedral shape, the maximal fraction of B5 sites appeared at around 1.8 nm. Similarly, Jacobsen have counted the relative number of B5-type sites on small Ru crystals and found a similar trend of B-5 fraction toward the crystal size [25]. It is therefore

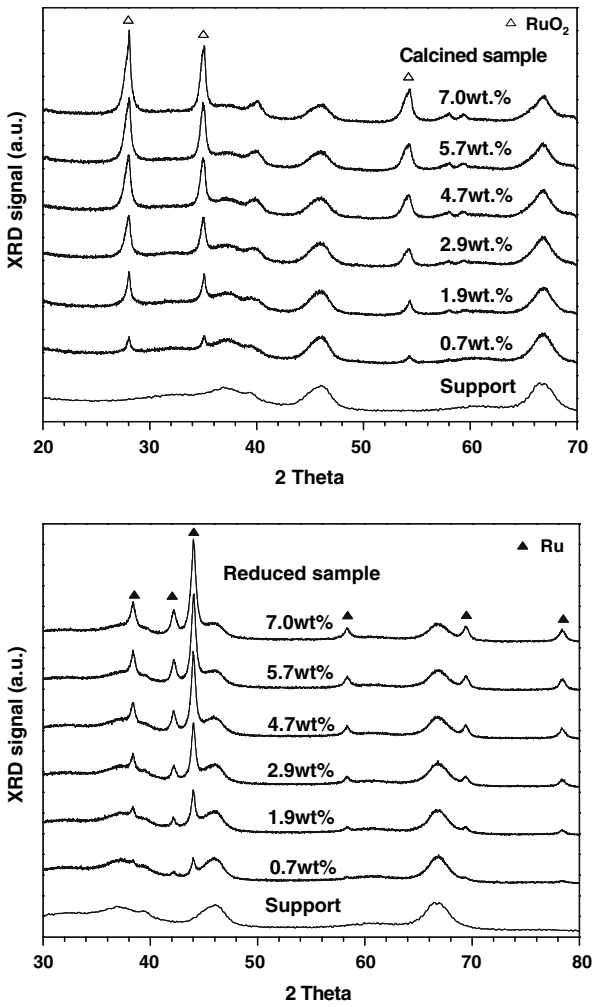

Fig. 3 XRD of all calcined and reduced Ru/Al_2O_3 catalysts

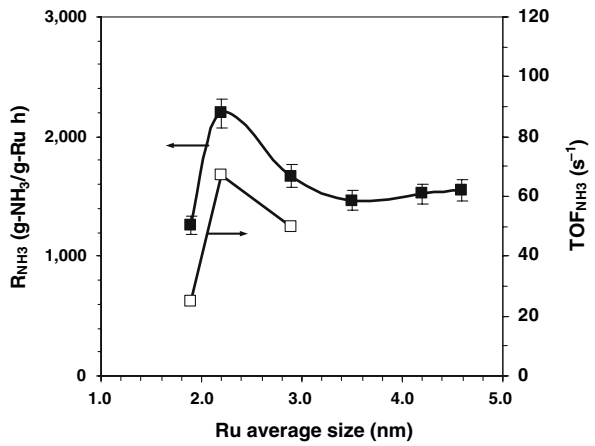

Fig. 4 Measured initial reaction rates (g_{NH_3} g_{Ru}^{-1} h^{-1}) and turnover rates (TOF_{NH_3}, s^{-1}) for NH_3 decomposition at 733 K over different Ru catalyst as a function of the average particle size (nm). Reaction conditions: 10.0 mg catalyst, d_p = 100–150 μm, dilution ratio = 1:50, total space velocity = 3,000,000 mL g_{cat}^{-1} h^{-1}, 15 kPa NH_3, balance He

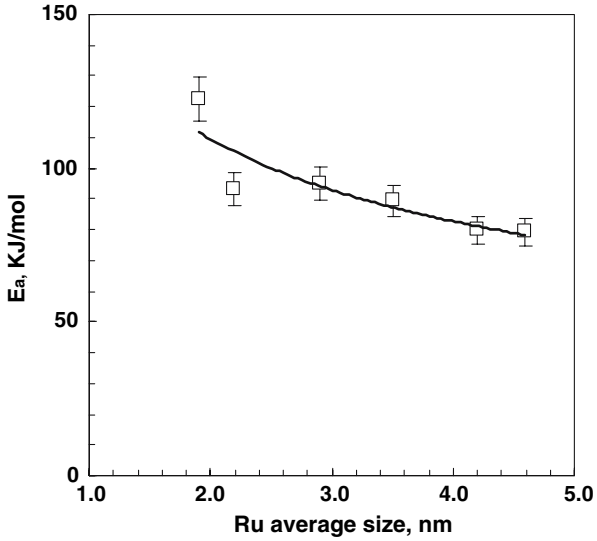

Fig. 5 Dependence of the Arrhenius activation energy for NH_3 decomposition on Ru particle size. Reaction conditions: 653–733 K, 10.0 mg catalyst, d_p = 100–150 m, dilution ratio: 1:50, total space velocity 3,000,000 mL g_{cat}^{-1} h^{-1}, 15 kPa NH_3, balance He

strongly suggested that B–5 sites of Ru act as the most active centers for NH_3 decomposition.

3.4.2 Reaction Orders of NH_3, N_2 and H_2

The dependencies of forward rate on partial pressures of NH_3, N_2 and H_2 were determined at 733 K and the reaction orders were determined. The forward rate was insensitive to P_{N_2} on each sample (not shown), indicating that the influence of N_2 on rate could be negligible. The pressure-dependent forward rates at 733 K were displayed in Figs. 6 and 7. As shown in Fig. 6, with varying P_{NH_3} in the range of 15–50 kPa and using He as balance, the rates over Ru catalysts monotonically increased. In contrast, with P_{NH_3} fixed at 15 kPa and P_{H_2} increased from 5 kPa to 40 kPa, the measured forward rates decreased. Therefore, similar positive orders with respect to NH_3 and negative order with respect to H_2 have been obtained for the Ru/Al_2O_3 catalyst studied. Such H_2 inhibition phenomenon agrees well with the previous studies on kinetic behaviors of Ru catalyst under the similar conditions. As seen in the inserts in Figs. 6 and 7, both reaction orders with respect to NH_3 and H_2 slightly changed with the decreasing Ru crystal size. It was indicated that the dependencies of forward rates on NH_3 and H_2 partial pressures were more significant over the Ru nanoparticles with low mean size.

3.4.3 Kinetics Model

All experimental kinetic data reported here could be well fitted by the Temkin–Pyzhev reaction equation as followed:

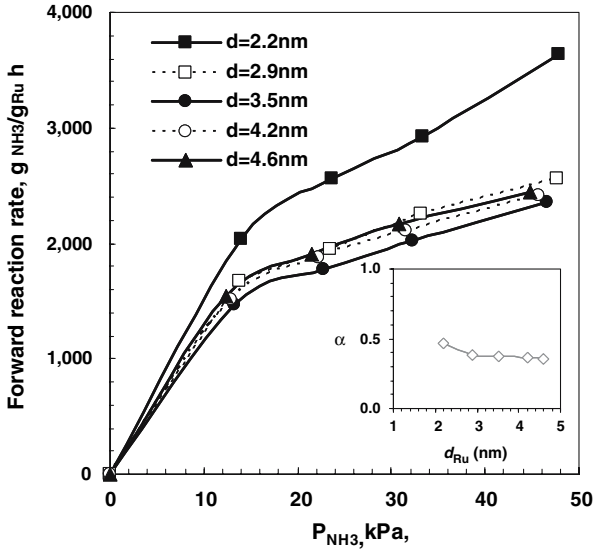

Fig. 6 Effects of NH_3 partial pressure on forward NH_3 reaction rate on Ru/Al_2O_3 catalysts. Reaction conditions: 10.0 mg of catalyst, 733 K, total space velocity 3,000,000 mL g_{cat}^{-1} h^{-1}, 15–50 kPa NH_3, balance He

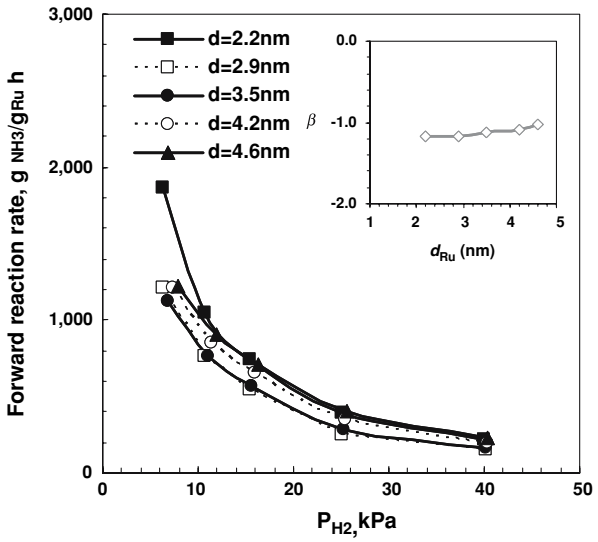

Fig. 7 Effects of H_2 partial pressure on forward NH_3 reaction rate on Ru/Al_2O_3 catalysts. Reaction conditions: 10.0 mg of catalyst, 733 K, total space velocity 3,000,000 mL g_{cat}^{-1} h^{-1}, 15 kPa NH_3, 5–40 kPa H_2, balance He

$$r_{\text{net}} = k\left[\left(\frac{P_{\text{NH}_3}^2}{P_{\text{H}_2}^3}\right)^{\beta} - \frac{P_{\text{N}_2}}{K_{\text{eq}}^2}\left(\frac{P_{\text{H}_2}^3}{P_{\text{NH}_3}^2}\right)^{1-\beta}\right] \quad (1)$$

$$k = A_{\text{app}} e^{-\text{E}_a/RT} \quad (2)$$

where, k (g_{NH_3} g_{Ru}^{-1} h^{-1} $atm^{-\beta}$) is the reaction rate constant, A_{app} (g_{NH_3} g_{Ru}^{-1} h^{-1} $atm^{-\beta}$) is the pre-exponential factor, E_a (kJ mol^{-1}) is the activation energy, K_{eq} (atm) is the equilibrium constant that obtained from the equation

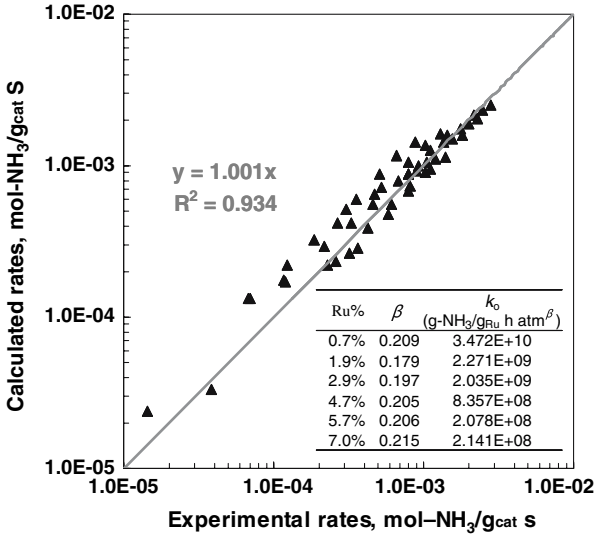

Fig. 8 Correlation between the experimental and calculated reaction rates (derived from the Temkin–Pyzhev expression as Eq. 2). Insert table: the derived kinetic parameters in the Temkin–Pyzhev expression

built by Harrison and Kobe [32]. Figure 8 presents the correlation between the experimental and calculated values at all experimental conditions. It is strongly suggested that the associative desorption of N* acts as the RDS for NH_3 decomposition over Al_2O_3 supported Ru nanoparticles. The derived kinetic parameters in the Temkin–Pyzhev expression for each sample were shown in the insert table in Fig. 8.

3.4.4 Relationship Between Particle Size Effect and Compensation Effect

The compensation phenomenon in numerous heterogeneous reactions takes the form of a sympathetic linear correlation between the observed parameters of the Arrhenius equation E_{app} and $\ln A_{app}$ for a series of related reactions or catalysts [33]. As evidenced in Fig. 9, a good linearity with regression coefficients (R^2) of 0.97 was observed in this plot of $\ln k_o$ versus E_a, indicating a convincing compensation effect for the NH_3 decomposition reaction over alumina supported Ru nanoparticles. Jacobsen have observed such compensation effect between apparent activation energies and pre-factors for the NH_3 synthesis reaction over a series of bimetallic alloys catalysts [34]. Under the assistance of theoretical calculation by DFT, the authors interpreted it by the shift of kinetic regime from one dominated by the rate of activation of reactants to a regime where the stability of the reaction products on the surface becomes increasingly important. For our case, all catalytic runs stayed in the compensation regime and, with decreasing cluster size of Ru, the NH_3

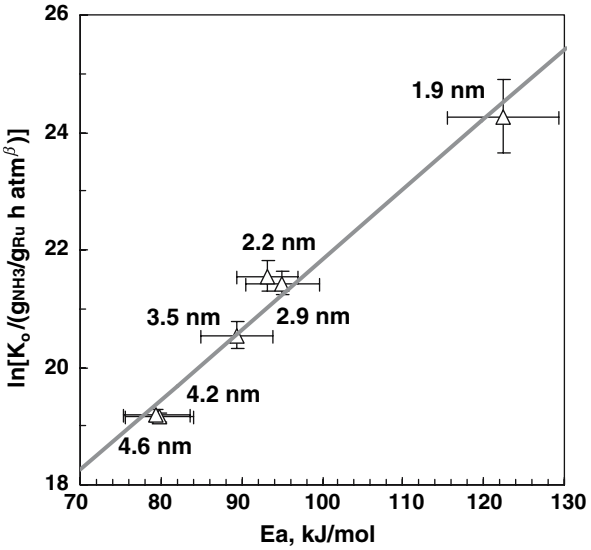

Fig. 9 Compensation effect for NH3 decomposition over Ru nanoparticles

decomposition process slowly approached to the coverage-limited regime.

4 Conclusions

A kinetic study of NH_3 decomposition over Ru nanoparticles with varying mean size, supported on a high-surface-area Al_2O_3, has been carried out at atmospheric pressure. Morphologies and crystallite sizes of Ru crystallites have been characterized by TEM. NH_3 decomposition is determined to be a structure-sensitive reaction that is best carried out over small Ru particles with size of 2.2 nm. Reducing particle size of Ru led to an increase in apparent activation energy and pre-exponential factor. This reaction proceeded according to the Temkin–Pyzhev mechanism, indicating that the recombinative desorption of surface nitrogen acted as the rate-determining step. In the present work, all catalytic runs remained in the compensation regime and the relationship between pre-exponential factor and activation energy was quantified. Decrease in average size of Ru nanoparticles slowly shifted the reaction towards the coverage-limited regime.

Acknowledgment This work was supported by National Basic Research Project of China (grant: 2005CB221400). We thank Professor Jianyi Shen of Nanjing University for his encouragement and insightful discussions. The contributions from Dr. Yanli He to experiments are also gratefully acknowledged.

References

1. Ertl G, Huber M (1980) J Catal 61:537
2. Hashimoto K, Toukai N (2000) J Mol Catal A 161:171
3. T-Rassi A (2002) Proceeding of the 2002 U.S. DOE hydrogen program review, NREL/CP–610–32405
4. Chellappa AS, Fischer CM, Thomson WJ (2002) Appl Catal A 227:231
5. Yin SF, Xu BQ, Zhou XP, Au CT (2004) Appl Catal A 277:1
6. Choudhary TV, Sivadinarayana C, Goodman DW (2001) Catal Lett 72:197
7. Ganley JC, Thomas FS, Seebauer EG, Masel RI (2004) Catal Lett 96:117
8. Yin SF, Zhang QH, Xu BQ, Zhu WX, Ng CF, Au CT (2004) J Catal 224:384
9. Boisen A, Dahl S, Nørskov JK, Christensen CH (2005) J Catal 230:309
10. Yin SF, Xu BQ, Ng CF, Au CT (2004) Appl Catal B 48:237
11. Bradford MC, Fanning PE, Vannice MA (1997) J Catal 172:479
12. Raróg W, Kowalczyk Z, Sentek J, Składanowski D, Szmigiel D, Zieliński J (2001) Appl Catal A 208:213
13. Raróg-Pilecka W, Szmigiel D, Kowalczyk Z, Jodzis S, Zieliński J (2003) J Catal 218:465
14. Raróg-Pilecka W, Szmigiel D, Komornicki A, Zieliński J, Kowalczyk Z (2003) Carbon 41:589
15. Li L, Zhu ZH, Yan ZF, Lu GQ, Rintoul L (2007) Appl Catal A 320:166
16. Szmigiel D, Raróg-Pilecka W, Miśkiewicz E, Kaszkur Z, Kowalczyk Z (2004) Appl Catal A 264:59
17. Yin SF, Xu BQ, Zhu WX, Ng CF, Zhou XP, Au CT (2004) Catal Today 27:27
18. Yin SF, Xu BQ, Wang SJ, Ng CF, Au CT (2004) Catal Lett 96:113
19. Tsai W, Weinberg WH (1987) J Phys Chem 91:5302
20. Egawa C, Nishida T, Naito S, Tamaru K (1984) J Chem Soc, Faraday Trans 80:1595
21. Tamaru K (1988) Acc Chem Res 21:88
22. Vitvitskii AI, Gaigei TP, Toporkova ME, Kiseleva EM, Melikhov EN (1991) J Appl Chem USSR 63:1883
23. Mariadassou GD, Shin CH, Bugli G (1999) J Mol Catal A 141:263
24. Mhadeshwar AB, Kitchin JR, Barteau MA, Vlachos DG (2004) Catal Lett 96:13
25. Jacobsen CJH, Dahl S, Hansen PL, Törnquvist E, Jensen L, Topsøe H, Prip DV, Møenshaug PB, Chorkendorff I (2000) J Mol Catal A 163:19
26. Hardeveld V, Montfoort V (1966) Surf Sci 4:396
27. Jedynak A, Kowalczyk Z, Szmigiel D, Raróg W, Zieliński J (2002) Appl Catal A 237:223
28. Zhang J, Xu HY, Jin XL, Ge QJ, Li WZ (2005) Appl Catal A 290:87
29. Zhang J, Xu HY, Ge QJ, Li WZ (2006) Catal Comm 7:148
30. Nazimek N (1984) Appl Catal 12:227
31. Romdhane YH, Bellamy B, Gouveia VD, Masson A (1988) Appl Surf Sci 31:383
32. Harrison RH, Kobe KA (1953) Chem Eng Proc 49:349
33. Liu L, Guo QX (2001) Chem Rev 101:673
34. Bligaard T, Honkala K, Logadottir A, Nørskov JK, Dahl S, Jacobsen CJH (2003) J Phys Chem B 107:9325